Verification and validation of linear gyrokinetic simulation of Alfvén eigenmodes in the DIII-D tokamak

D. A. Spong,[1,a)] E. M. Bass,[2] W. Deng,[3] W. W. Heidbrink,[3] Z. Lin,[3] B. Tobias,[4] M. A. Van Zeeland,[5] M. E. Austin,[6] C. W. Domier,[7] and N. C. Luhmann, Jr.[7]
[1]*Oak Ridge National Laboratory, Oak Ridge, Tennessee 37830, USA*
[2]*Department of Physics, University of California, San Diego, California 192093, USA*
[3]*Department of Physics and Astronomy, University of California, Irvine, California 92697, USA*
[4]*Princeton Plasma Physics Laboratory, Princeton, New Jersey 085430, USA*
[5]*General Atomics, San Diego, California 92121, USA*
[6]*Institute for Fusion Studies, University of Texas, Austin, Texas 78712, USA*
[7]*Department of Electrical and Computer Engineering and Department of Applied Science, University of California, Davis, California 95616, USA*

(Received 30 April 2012; accepted 7 August 2012; published online 20 August 2012)

A verification and validation study is carried out for a sequence of reversed shear Alfvén instability time slices. The mode frequency increases in time as the minimum (q_{min}) in the safety factor profile decreases. Profiles and equilibria are based upon reconstructions of DIII-D discharge (#142111) in which many such frequency up-sweeping modes were observed. Calculations of the frequency and mode structure evolution from two gyrokinetic codes, GTC and GYRO, and a gyro-Landau fluid code TAEFL are compared. The experimental mode structure of the instability was measured using time-resolved two-dimensional electron cyclotron emission imaging. The three models reproduce the frequency upsweep event within ±10% of each other, and the average of the code predictions is within ±8% of the measurements; growth rates are predicted that are consistent with the observed spectral line widths. The mode structures qualitatively agree with respect to radial location and width, dominant poloidal mode number, ballooning structure, and the up-down asymmetry, with some remaining differences in the details. Such similarities and differences between the predictions of the different models and the experimental results are a valuable part of the verification/validation process and help to guide future development of the modeling efforts.
 [http://dx.doi.org/10.1063/1.4747505]

I. INTRODUCTION

Fully self-consistent simulation of energetic particle turbulence and transport in burning plasmas must incorporate three new physics elements: kinetic effects of thermal particles at the thermal ion gyro-radius (*micro* scale), nonlinear interactions of many *meso* scale (energetic particle gyro-radius) shear Alfvén waves induced by the kinetic effects at the *micro* scale, and *meso-micro* couplings of the micro-turbulence and shear Alfvén wave turbulence. The large dynamical ranges of spatial-temporal processes further require global simulation codes to be efficient in utilizing massively parallel computers. Therefore, the studies of energetic particle physics in the burning plasma regime require a new approach using gyrokinetic turbulence simulation. In this paper, we document progress in the verification and validation of the simulation of Alfvén eigenmodes using the advanced tokamak regime of the DIII-D experiment as a reference case.

Verification is defined as an assessment of the fidelity of the computational model to the underlying analytical conceptual model, while validation is an evaluation of the degree to which the computational model represents experimental reality.[1–3] Although the codes used in this paper are comprised of components that have either been previously verified or are well-tested computational science library functions, the simulation problem examined here and those of most interest typically do not have analytical solutions and cannot be directly verified in the traditional sense. Therefore, code-to-code comparisons (benchmarking) of three independently developed codes are used here for the verification step; as these codes use somewhat different physics models and solution methods, the verification process is approximate. The validation step is based on comparisons to the DIII-D experiment; this is also necessarily an approximate, ongoing process since there are hidden/unmeasured variables (e.g., time-dependent q-profile, fast ion distribution function) that impact the predictions and for which the computational models must currently make assumptions. A hierarchy of different comparisons is included. First, two independent gyrokinetic models are used: gyrokinetic toroidal code (GTC), which is a gyrokinetic particle model, and GYRO, which is a gyrokinetic Eulerian (continuum) model. Next, to complete the verification step, these are compared with a gyro-Landau fluid model, TAEFL. Finally, for the validation component, all three models are compared with DIII-D experimental results for beam-driven Alfvénic instabilities with time-varying frequencies.

The advanced tokamak regime is characterized by a central reversed shear in the safety factor profile with an off-axis minimum and is of significant interest for future fusion

a)Electronic mail: spongda@ornl.gov.

devices. This profile choice provides a good alignment of the bootstrap current with total current, leading to the possibility of steady-state operation with low recirculating power and high β_{poloidal}.[4] The shear reversal provides enhanced stability to ballooning and neoclassical tearing instabilities[5] and has been observed to facilitate the formation of internal transport barriers.[6] Finally, hollow current profiles can improve wall stabilization of low-n kink modes.[7] Such operational modes have been produced on DIII-D,[8] JET,[9] JT-60U,[10] ASDEX-Upgrade,[11] and C-Mod[12] and are important components for future ITER scenario planning.[13]

However, off-axis minimum q-profiles provide conditions that are favorable to the existence of energetic particle driven reversed shear Alfvén eigenmode (RSAE) instabilities. These modes are typically localized around the minimum of the q-profile, dominated by a single poloidal mode with $m/n \approx q_{min}$, although remaining globally non-resonant ($k_{\|} \neq 0$). They have been seen on a range of tokamaks[14–19] and are often associated with a frequency that rises or falls in time. This frequency change, often referred to as an Alfvén cascade,[20,21] is attributed to the evolution of the equilibrium q-profile and is not related to the nonlinear phase-space effects[22] that are attributed to the more rapidly changing "chirping-frequency" Alfvén instabilities. RSAE instabilities have been associated with a loss and redistribution of energetic beam ions.[23,24,33,34] Recently, electron cyclotron emission imaging (ECEI) measurements[25,26] have been carried out for energetic particle-driven instabilities on DIII-D. These have provided unprecedented new information on the two-dimensional mode structure of both RSAE and toroidal Alfvén eigenmode (TAE) instabilities. The availability of such information has greatly increased the possibilities for theory/experiment validation activities and has provided additional motivation for the work reported in this paper.

Assessing the importance of the RSAE instability for future advanced, steady-state tokamak regimes will require the development of reliable and accurate simulation methods that can predict its threshold, mode structure, time variation, nonlinear saturation levels, and impact on fast ion confinement. The purpose of this paper is to provide an initial test of three models that are under development in the gyrokinetic simulation of energetic particle turbulence and transport (GSEP) SciDAC project.[27] Two of these models, GTC and GYRO, are based on gyrokinetic models that advance the fast ion distribution in five-dimensional phase space, coupled with similar models for the thermal plasma species. This approach can provide a comprehensive physics description for the energetic particle (EP)-driven modes, as well as their damping and interaction with the thermal plasma. The third model, TAEFL, is derived by taking moments of the gyrokinetic equation, but uses Landau fluid closures to incorporate the phase-mixing physics required for resonant fast ion instabilities. This leads to a computationally efficient model for simulating EP instabilities involving coupled partial differential equations in three-dimensional configuration space, which can be calibrated against the more fundamental gyrokinetic methods. This paper represents the first time such a hierarchy of models has been compared for Alfvén instabilities. No such comparisons have previously been made between independent gyrokinetic models. An earlier study[28] was made for a DIII-D TAE mode between perturbative, hybrid gyrokinetic models (i.e., only the EP component was gyrokinetic) and Landau-fluid models, but gave results that differed more strongly between models than those presented here.

In the following paper, the specific time slice and DIII-D discharge that is modeled will first be discussed. The profiles and reconstruction methodology used are specified. Next, the three theoretical models are briefly described; more detailed characterizations of each model will be contained in separate publications. Following this, the predictions of the models with respect to frequency, growth rate, and mode structure are presented as the q_{min} (for a fixed profile shape) evolves. Next, data from ECE imaging that is relevant to the modeling is presented, followed by a conclusion section. We find good agreement between the models and experiment on a number of features: reproduction of the frequency upsweep event (average predicted frequency from the 3 codes is within $\pm 8\%$ of the measurements, individual codes are within $\pm 18\%$); prediction of growth rates that are consistent with the observed spectral line widths; and mode structures that qualitatively agree with respect to radial location, dominant poloidal mode number, and ballooning structure variation as q_{min} changes. There are remaining differences in the radial variation of the up-down asymmetry (as measured by the radial phase variation). This topic, along with further refinement of the frequency and growth rate variations, motivates future research and development in the modeling efforts.

II. DIII-D REVERSED SHEAR TEST CASE AND EXPERIMENTAL PROFILES

For the code comparison, a test case is chosen from DIII-D discharge #142111. This is a reversed shear discharge with many unstable RSAE and TAE modes present. The discharge is similar to earlier discharges,[29–31] with radial eigenfunctions that resemble mode structures calculated by the ideal MHD code NOVA.[32] These operating conditions lead to strong flattening of the fast-ion profile.[33,34] Recent papers discuss measurements of beam ion losses[35,36] and of the two-dimensional (toroidal slice) mode structure[25,26] in discharge #142111.

A time slice ($t = 725$ ms) with excellent diagnostic coverage is selected for the code comparison. The plasma equilibrium is carefully reconstructed using a multi-step process. The first step is an equilibrium reconstruction by the EFIT code,[37] based on magnetic and motional Stark effect (MSE)[38] data. Next, measurements of electron and carbon density and of electron and ion temperatures are mapped onto the equilibrium and the profiles are fit. An initial calculation of the classical fast-ion pressure profile $p_{f,classical}$ is computed next. Using the assumption of quasi-neutrality, the thermal pressure profile p_{th} is inferred from the fitted n_e, n_C, T_e, and T_i profiles and the calculated fast-ion density. The true pressure profile is assumed to lie between p_{th} and $p_{th} + p_{f,classical}$, and the equilibrium is recomputed by EFIT. The calculated equilibrium is compared to a radial array of

ECE measurements to ensure that T_e is a flux function. Additionally, the sequence of RSAE activity known as "grand cascades"[39] is used to identify rational values of q_{min}. With the assumption that the RSAE eigenfunction peaks near the minimum q radius, the radial location of q_{min} is also known experimentally. The reconstructed equilibrium agrees well with all of the available data: magnetics, MSE, thermal pressure, ECE, and RSAE integer crossings.

The kinetic profiles obtained by this procedure are shown in Figs. 1(a) and 1(b). The estimated uncertainty in the electron and thermal ion temperatures and densities is about 5 and 10%, respectively. For the simulations in this paper, a modification of the original thermal plasma density profiles has been made and is reflected in the profiles of Fig. 1(a); the original profiles had steep edge gradient pedestal regions. In some cases these drove edge-localized modes unrelated to the RSAE/TAE modes that are the subject of this study. Since the modes examined in this paper are localized well to the interior of this pedestal region, this modification in the thermal density profiles should not significantly affect their characteristics. The q-profile is shown in Fig. 1(e). The value and radial location of q_{min} is known quite accurately but the magnetic shear is more uncertain, especially near the magnetic axis, where q_0 has an uncertainty of $\sim$10%. At large minor radius, the q-profile is accurately determined by the combination of magnetic and MSE data. The q-profile shown in Fig. 1(e) is for $q_{min} = 3.18$. In the code comparisons (Sec. IV), this profile is translated up and down, keeping the same shape, in order to cover the range of $q_{min} = 3.1$–3.32 used in the theoretical modeling. We note that the actual experimental q profiles may change shape during the frequency sweep and this will influence the accuracy of the predictions; time-resolved q profile reconstructions within the sweep interval were not available.

The plasma shape for this discharge is an up-down symmetric oval (see Fig. 2 of Ref. 35 for an illustration). At

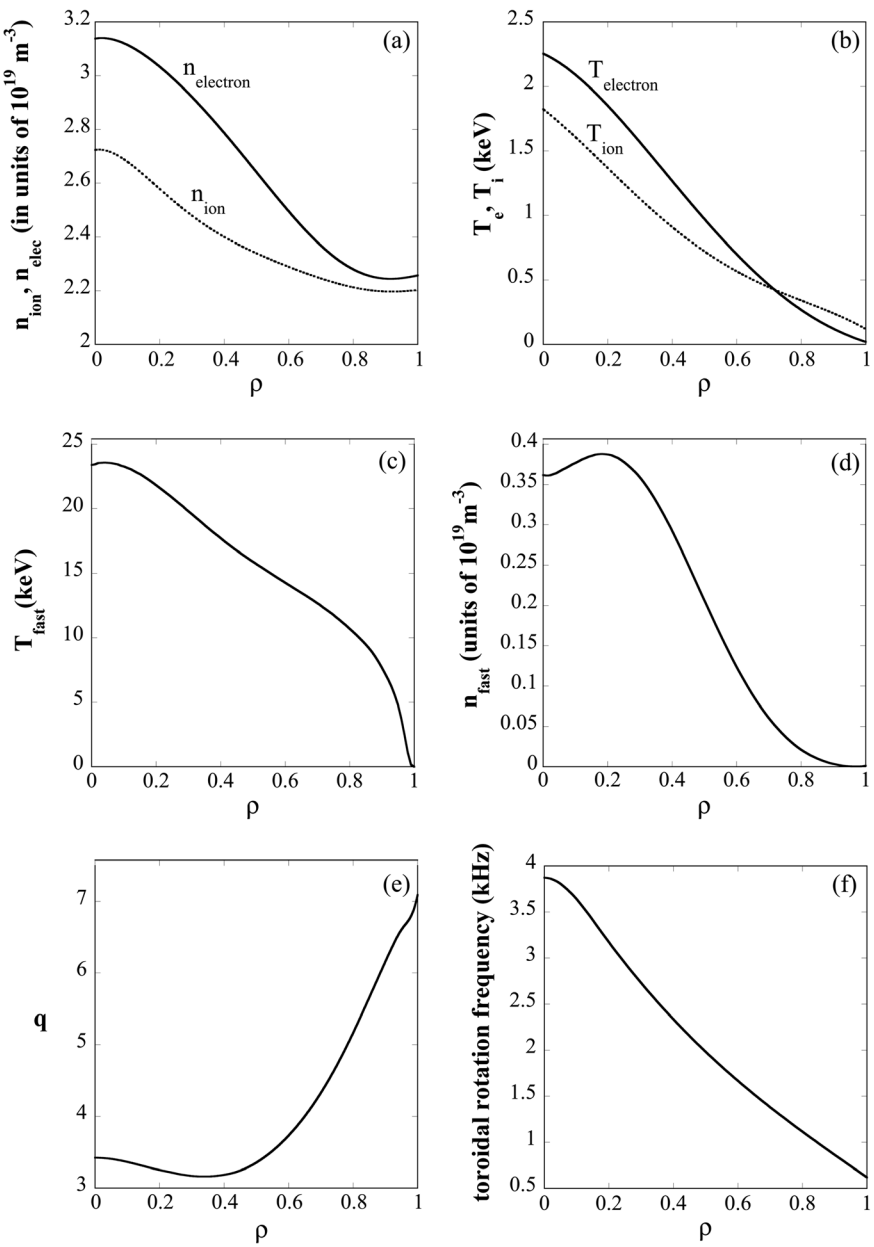

FIG. 1. Profiles used in the calculations: (a) electron and ion densities; (b) electron and ion temperatures; (c) effective fast ion temperature; (d) fast ion density; (e) q-profile and (f) toroidal rotation velocity (not included in simulations).

725 ms, the plasma current is 0.9 MA, the toroidal field is 2.0 T, the elongation is $\kappa = 1.6$, and the triangularity is $\delta = 0.05$. Empirically, the Alfvén activity is insensitive to precise details of the plasma shape.

The instabilities are driven by injection of 4.6 MW of deuterium neutrals at 75–81 keV. Near-tangential injection is employed, with 82% of the neutrals injected in the co-current direction and 18% in the counter-current direction. The plasma is driven well beyond marginal stability, which occurs for beam powers less than half of this value. As a result, the fast ion distribution function is far from its classical value, and substantial uncertainty exists concerning its precise form. At the selected time slice, the neutron rate is about 2/3 of the classically predicted value, and the central fast ion density inferred from a vertical fast ion D alpha measurement is about 1/3 of the classical value.[35,36] In velocity space, the distribution function is expected to approximate an anisotropic slowing-down distribution. Figure 2 shows the classical distribution function computed by the TRANSP NUBEAM (Ref. 40) module. The distribution consists primarily of fast ions that circulate in the co-current direction. In this regime, spatial transport is probably dominated by diffusion associated with multiple wave-particle resonances with small amplitude modes.[23,24] The actual spatial gradient near q_{min} is much flatter than the classical prediction but is quite uncertain. For the code comparisons (Sec. IV), the fast ion distribution is approximated by an isotropic Maxwellian with the temperature and spatial profiles shown in Figs. 1(c) and 1(d). The effective temperature profile is obtained from classical deposition calculations while the fast ion pressure profile and density is inferred by subtracting the thermal pressure from the re-fitted equilibrium pressure profile while maintaining quasi-neutrality. Although this model is a crude approximation to the true distribution function, it does mimic the resonances and spatial gradients that drive the RSAE instabilities.

Basic identification of the instabilities utilizes a combination of magnetic, interferometer, and ECE data supplemented by NOVA calculations. The entire pattern of observed instabilities is sorted into RSAEs and TAEs of different mode numbers, as illustrated in Figs. 2 and 3 of Ref. 31. Many toroidal mode numbers are measured by a toroidal array of magnetic coils and are corroborated by the time evolution of the frequency at the Alfvén cascades. For the code comparison, an $n = 3$ RSAE with excellent ECEI data is selected. The frequency in the laboratory frame is known accurately but the frequency in the plasma frame is affected by toroidal rotation [Fig. 1(f)]. The measured rotation profile is for carbon but the expected difference between the carbon and bulk rotation is small for these conditions. At the q_{min} surface, the toroidal rotation is 2.6 ± 0.3 kHz and the Doppler shift frequency offset for an $n = 3$ mode is approximately 8 kHz. The experimental mode amplitude is fairly modest, $\delta T_e/T_e \simeq 1\%$.

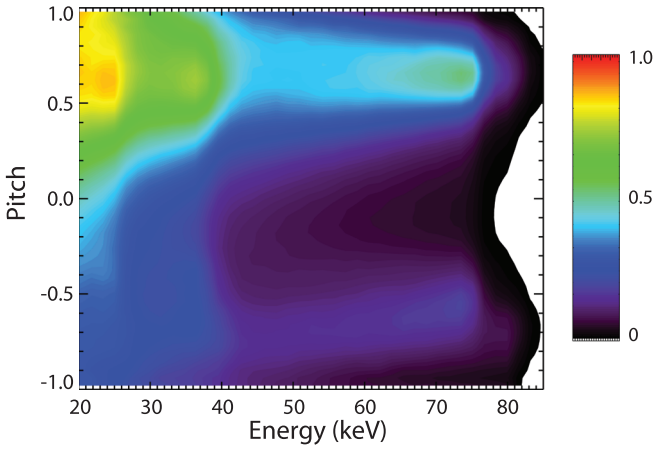

FIG. 2. NUBEAM calculation of the volume-average, classical fast-ion distribution function in discharge #142111 near 725 ms. Positive pitch $v_{\|}/v$ is in the co-current direction.

III. DESCRIPTION OF THE MODELS

A. GTC

The gyrokinetic toroidal code (GTC)[41] is a full torus gyrokinetic particle-in-cell (PIC) code capable of both δf and full-f simulations, including kinetic electrons, electromagnetic fluctuations, general toroidal geometry, experimental plasma profiles, multiple ion species, neoclassical effects, radial electric fields, plasma rotations, and external antenna. In the current δf simulation, the equilibrium distribution function f_0 for any species is a Maxwellian in the velocity space. The perturbed distribution δf for either thermal ions or energetic ions is carried by marker particles. Each marker particle's evolution in the phase space follows the equations of gyro-center motion[42] and its weight ($\delta f/f_0$) evolution follows the gyrokinetic equation.[43] The electrons are simulated using a fluid-kinetic hybrid model.[44] In the lowest order, i.e., adiabatic limit, the electrons are described by the fluid continuity equation, which comes from integrating the drift-kinetic equation over the velocity space. Higher order corrections, i.e., kinetic effects, are obtained by solving the non-adiabatic part of the electron distribution function δh_e from the drift-kinetic equation using the PIC method. The electromagnetic field is solved using the gyrokinetic Poisson's equation[45] and Ampère's law. GTC was originally developed for simulations of micro-turbulence[46,47] and has recently been extended for simulation of energetic particle physics[48–51] and kinetic magnetohydrodynamic (MHD) processes with equilibrium current.[52] The gyrokinetic formulation in GTC has been proven to recover all the linear ideal MHD physics including kinetic ballooning modes, shear Alfvén waves, current-driven modes, and pressure-driven modes.[52]

While GTC has the option to treat ions drift-kinetically and the option to treat electrons adiabatically, simulations in this work are performed with gyrokinetic thermal ions and fast ions and with drift-kinetic electrons. GTC calculates the polarization current[53] from both thermal and energetic ions, but makes an approximation that introduces an error to the total polarization current on the order of $(n_{fast}/n_{electron})(k_\perp \rho_{fast})^2/[1 + (k_\perp \rho_{fast})^2]$, which is very small for the simulations reported in this paper. Equilibrium current is included in these simulations.[52] Collision and rotation effects are turned off. The simulation domain is approximately $0.1 \le \rho \le 0.9$, where ρ is the square root of the normalized

toroidal flux. The real space grid size is about $\Delta\rho/\rho_i \sim \rho\Delta\theta/\rho_i \sim 1.3$, where ρ_i is the thermal ion gyro-radius at the q_{min} surface. The time grid size is $\Delta t = 0.068 v_{A0}/R_0$, where v_{A0} is the on-axis Alfvén speed and R_0 is the major radius. Each of the three species has 50 marker particles per cell. These parameters are chosen based on convergence tests.[54] A toroidal mode filter is used to select only the $n = 3$ mode.

B. GYRO

GYRO solves the gyrokinetic equations for each kinetic species on a continuum, field-aligned grid. All species are treated kinetically, with each having a separate grid spanning the five-dimensional gyrokinetic phase space. While GYRO can operate fully electromagnetically, including magnetic compressibility, only the electrostatic potential ϕ and the field-line-bending piece of the vector potential $A_\parallel$ are tracked in the present simulations. The toroidal degree of freedom is treated spectrally, allowing for efficient calculation of linear eigenmodes (only one toroidal mode number). GYRO can solve using either a local (constant profiles) or global (varying profiles) model. This global eigenmode study preserves full profile variation. All species have an isotropic Maxwellian velocity-space equilibrium distribution function for each value on the real-space grid. GYRO uses the δf approximation, meaning that perturbations are assumed small (order ρ_*) in the ordering. A high-n ballooning mode approximation ($k_\parallel \ll k_\perp$) is also employed. In this limit, poloidal and radial variation of the "envelope" function is assumed slow compared to the variation due to the rapidly fluctuating ($\partial/\partial\theta \approx nq$) eikonal. For the present $n = 3$ case, the discarded term is confirmed a posteriori to be at worst about 3% of the preserved eikonal term across the domain for all tested cases. Only the slowly varying envelope is tracked in a GYRO simulation, enabling a comparatively coarse poloidal grid. For a complete description of the GYRO discretization and solution schemes, see Ref. 55.

The present linear simulations span $0.15 \leq \rho \leq 0.80$. All fluctuations, including potential fields and distribution function perturbation, are constrained to be zero at the simulation boundaries. The RSAE is radially localized near the q_{min} surface, with lesser sidebands extending to larger ρ. In cases where the sidebands extend to the simulation boundary, rapid eigenfunction dropoff should be interpreted as an artifact of the boundary condition. There are three gyrokinetic species: electrons, thermal deuterium, and beam deuterium. Accurate treatment of the three disparate Larmor scales represented requires more computational time in the solution for the fluctuating fields but ensures the ion polarization current and other finite Larmor radius effects are self-consistent with the chosen Maxwellian distributions. The continuum grid for each species has 300 radial gridpoints, 20 along θ, 8 in pitch angle (4 trapped, 4 passing), and 8 in energy (rescaled by local temperature). One toroidal mode number ($n = 3$) is tracked in all cases. Results presented here are from GYRO's direct linear eigenvalue solver.[56] While a spectrum of unstable eigenmodes is obtained with this solver, we present only one eigenmode in each case. The mode shown is chosen to best match the leading eigenmode from the other two codes in the study and is in most cases the leading GYRO eigenmode as well. Collision and rotation effects are neglected in all results.

C. TAEFL

TAEFL is an initial value code based on fast ion Landau closure techniques that were developed and verified[57,58] with analytic TAE growth and damping results. Two moment equations (density and parallel momentum) are used for the fast ion species; the fast ion parallel momentum equation closure was derived using techniques[59] that incorporate Landau growth/damping. The use of two moments implies that the plasma dispersion relation is approximated by a two-pole fit. The parameters of the fit are adjusted to improve the accuracy of the fast ion closure; higher order closures are under development. The mode structures in TAEFL are represented using Fourier expansions in poloidal and toroidal angles and finite differences in the flux (radius-like) coordinate, and the full volume from the magnetic axis to the outermost flux surface ($0 \leq \rho \leq 1$) is simulated. The Fourier representations are essential for performing the Landau closure since they allow the parallel wavenumber to be expressed as a scalar rather than as a differential operator. The thermal plasma is represented by a single fluid reduced MHD model, which includes geodesic/acoustic couplings. Four evolution equations are used for the thermal plasma, consisting of the parallel component of the vorticity equation (derived from $B\cdot\nabla\times$ operating on the momentum balance equation), Ohm's law, the density convection equation, and thermal ion parallel momentum equation. A purely ideal MHD model is used here with no collisional dissipation (i.e., the diffusivities, viscosities, resistivity are set to zero). The ideal MHD model is also augmented with a thermal ion FLR term (for coupling to the kinetic Alfvén wave) and an ion/electron Landau damping term. TAEFL uses implicit time stepping[60] for linear calculations and can be run for sufficiently long physical times that only a single (most unstable) mode dominates. For the calculations presented here, TAEFL was run with 400 radial grid points and 20 (m,n) pairs in the Fourier series used to represent the mode structures.

IV. COMPARISON AND DISCUSSION OF THE SIMULATION RESULTS

The three codes described above have been applied to an $n = 3$ Alfvén instability in DIII-D as the minimum in the q-profile changes from 3.32 to 3.1 in order to simulate the observed frequency sweep dynamics. All of the codes find unstable modes over this range of q-profiles. A frequency upsweep similar to that observed experimentally is predicted, and associated changes in mode structure are found. The rate of change in the q-profile (inferred from the frequency sweep rate) is small compared to either the instability growth rate or real frequency; this motivates a linearized, quasi-static (time sequence of equilibria) analysis, as is used here. As mentioned in Sec. II, this comparison is also based on the assumption that the q profile retains the same shape and uniformly drops in magnitude during the sweep event; shape changes that may be present in the actual profiles will impact

the accuracy of the modeling. Our comparisons among codes follow the hierarchy, gyrokinetic-particle (GTC) to gyrokinetic-Eulerian (GYRO) followed by gyrokinetic to gyro-Landau fluid (TAEFL), and finishing with comparison to experiment. The results from these three models are plotted and compared in Figures 3 through 5. Figure 3(a) plots the frequency and growth rate variation as q_{min} decreases. Fig. 3(b) displays an ECEI mode structure associated with the time where q_{min} passes through 3.22. The different models show similar trends in that the frequency rises with decreasing q_{min}, reaching a maximum around $q_{min} = 3.16$–3.18 and then drops off slightly. This drop-off is associated with a transition in the mode structure from a single dominant poloidal mode (RSAE-like) to increasingly coupled adjacent poloidal modes (TAE-like). In Fig. 3(a) the experimentally measured frequency has been transformed into the plasma reference frame by subtracting 8 kHz in order to approximately take into account the Doppler shift of an $n = 3$ mode in the presence of the toroidal rotation velocity of Fig. 1(f); none of the simulations directly take into account a toroidal rotation of the background plasma for the studies presented here. Also, the TAEFL frequencies have been shifted upward by 5 kHz, which is an estimate of the thermal ion diamagnetic frequency at the q_{min} surface. This is done to place the TAEFL results, which do not include thermal ion diamagnetic flows, on a similar footing with the GTC and GYRO models, which do include such flows implicitly in the guiding center transformation. The predicted real frequencies fall within about a ± 10% window of each other and a ± 18% window from the experimental observations. This can be attributed to a number of reasons: all simulations use Maxwellian distribution function for the fast ions, the simulations do not directly take into account plasma rotation or radial electric field effects, there remain uncertainties in the profiles, and the simulations include only a single thermal ion species. All three codes reproduce the frequency upsweep and down-sweep seen in the experimental spectrogram. The frequency deviations between codes can be attributed to the differences in the thermal plasma models, which determine the MHD spectrum. GTC is a fully electromagnetic model with gyrokinetic ions and drift kinetic electrons; GYRO treats all species gyrokinetically but retains only fluctuations in the electrostatic potential and field-line-bending component of the vector potential; TAEFL is based on a reduced MHD model, augmented with sound wave dynamics. The growth rates are relatively constant with a weak minimum near where the real frequency reaches its maximum. The TAEFL growth rates are also somewhat higher than those of GTC or GYRO. This can be related to the different damping effects that are present in the models. TAEFL includes lowest-order thermal ion FLR (radiative damping) and a perturbative model for electron/ion Landau damping. The gyrokinetic models also include FLR effects of thermal and fast ions and kinetic representations of radiative damping, and thermal ion Landau damping, in addition to continuum damping, electron damping, and driving by thermal plasma pressure gradients.[54] In principle, fast-ion FLR effects in the future can be included in the TAEFL model. The dispersion among growth rates from the different models can also be related to the differences in real frequency and the sensitive dependence of the wave-particle resonance condition on this frequency. This is especially important for the RSAE regime ($q_{min} > 3.15$) where a single (m,n) dominates the parallel wave number. As can be seen, RSAE growth rates become similar between the separate codes when the real frequencies match ($q_{min} \sim 3.3$ for TAEFL and GYRO; $q_{min} \sim 3.2$ for GTC and GYRO). Also, in the TAE regime ($q_{min} \sim 3.1$) the growth rates begin to converge as the real frequencies merge together.

Figures 4 and 5 show the mode structures at 3 different q_{min} values for the three codes. Figure 4 shows the absolute value of the potential functions as a function of poloidal

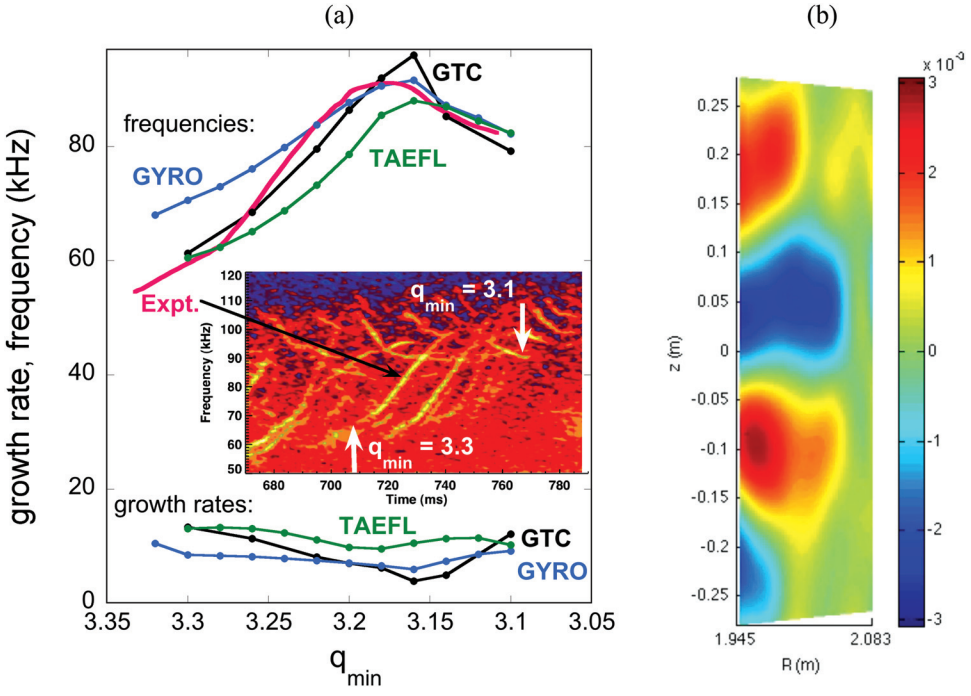

FIG. 3. (a) Variation of real frequency and growth rate with q_{min} among the three models and the experimental frequency variation; (b) mode structure measured with ECEI for $q_{min} = 3.22$ (time = 733.5 ms).

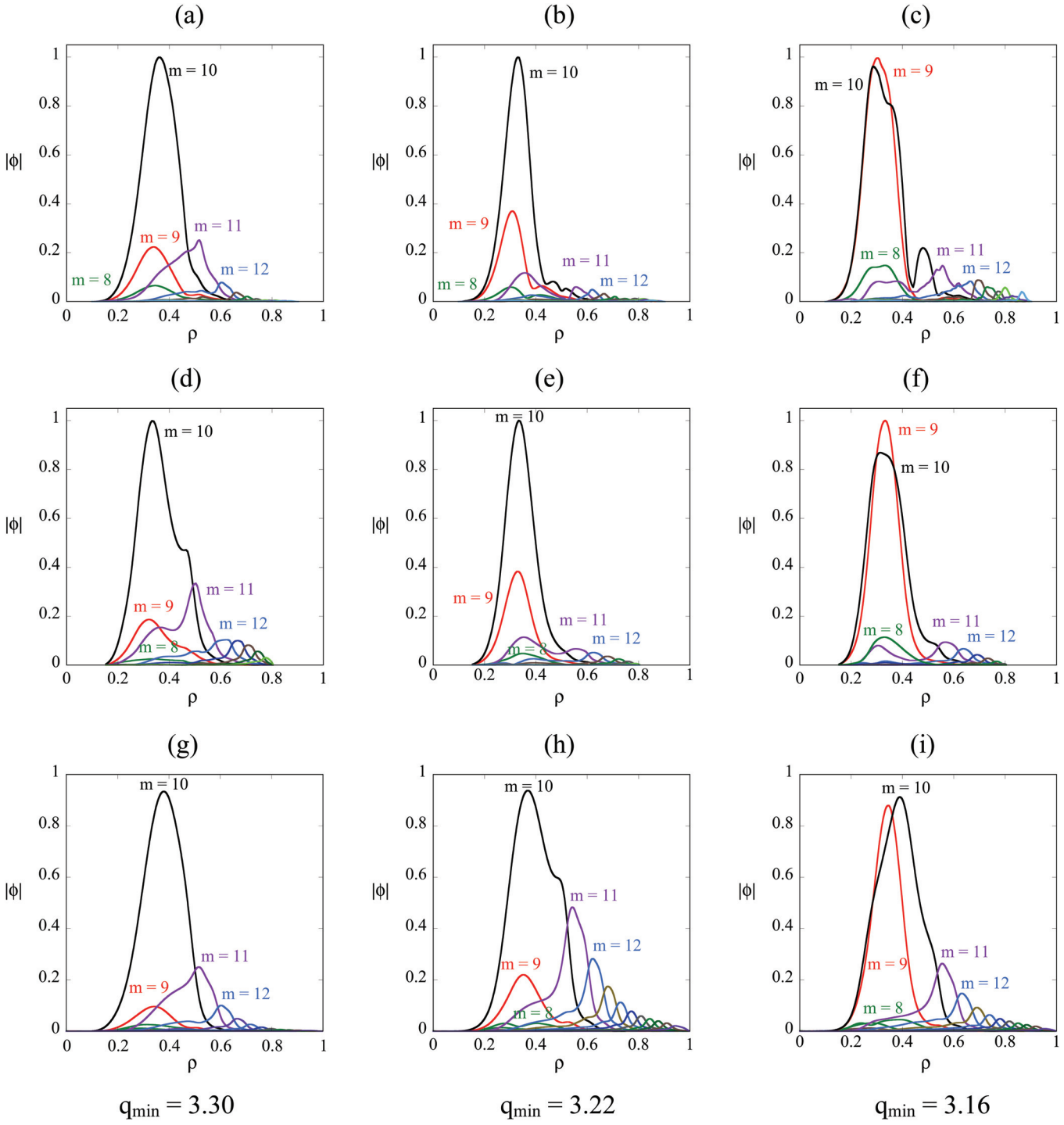

FIG. 4. Fourier eigenmode harmonics of the potential function from the 3 codes at 3 q_{min} values: (a), (b), (c) are from GTC; (d), (e), (f) are from GYRO; and (g), (h), (i) are from TAEFL. In each case, the figures going from left to right are for $q_{min} = 3.30$, 3.22, and 3.16.

mode number and radius (square-root of toroidal flux). Since these are linear calculations, all results have been normalized to unity for the dominant mode. As can be seen, the relative amplitudes of the $m = 9$–12 radial amplitudes change with q_{min}; this change is reasonably consistent across the three models. For example, all codes show that at $q_{min} = 3.22$ and 3.33 the $m = 10$ mode dominates while at $q_{min} = 3.16$ the $m = 9$ and 10 become more closely coupled. GTC and GYRO agree particularly well in both m-harmonic amplitudes and widths. The TAEFL amplitudes generally have a somewhat broader radial structure than GTC or GYRO and show a stronger coupling to the higher poloidal numbers (i.e., $m = 11$–20). This may be due to the different methods used in evaluating the damping physics. This point is illustrated by relative agreement in harmonic magnitude between the two gyrokinetic codes GTC and GYRO despite different cutoff radii.

Figure 5 displays the two-dimensional (at a constant toroidal angle) eigenmode structure from the three codes. The mode structures qualitatively agree with respect to radial

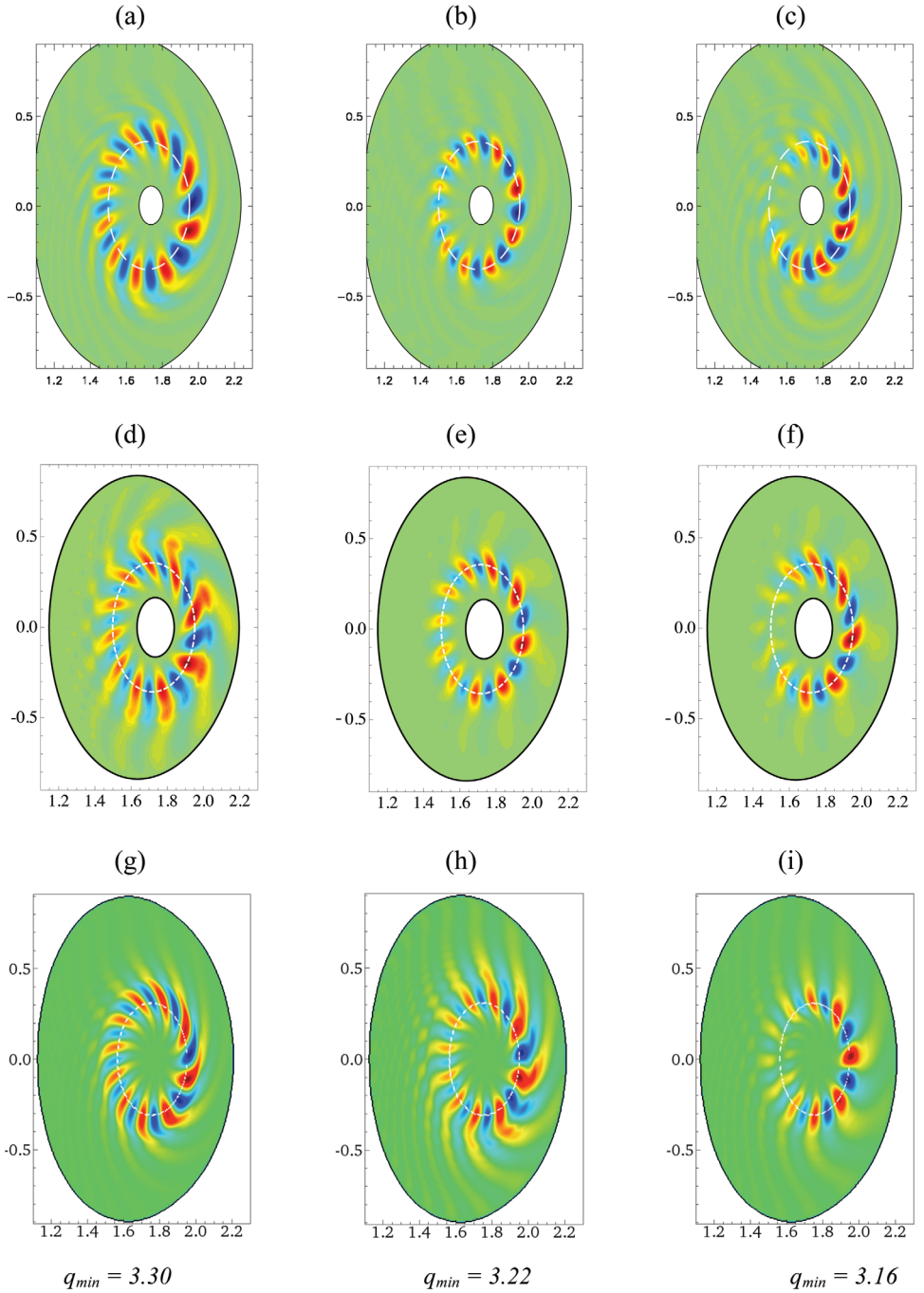

FIG. 5. Two-dimensional eigenmode structures from the 3 codes at 3 q_{min} values: (a), (b), (c) are from GTC; (d), (e), (f) are from GYRO; and (g), (h), (i) are from TAEFL. In each case, the figures going from left to right are for $q_{min} = 3.30$, 3.22, and 3.16.

location and width, ballooning structure, and the up-down asymmetry. The main differences are in the radial extent of the mode structure (as in Figure 4, TAEFL tends to predict more radially extended modes). Also, GYRO shows a reversal of the radial twist direction outside of a certain radius in all cases; this feature is less prevalent or absent in the other two models. Such effects can be highly sensitive to the model that is used. Near q_{min}, where the modes are strongest, the similar models of GTC and GYRO predict mode widths (also seen in Fig. 4) and pattern orientations in good agreement.

An important feature of the mode structures in Fig. 5 is the marked up-down asymmetry or poloidal twist that may be characterized by variation in the phase of the mode along a radial chord.[25] Since the underlying equilibria are up-down symmetric and no plasma flows or radial electric fields are included, this characteristic can be attributed mostly to fast ion diamagnetic effects. It has been verified in all three codes that the direction of twist is reversed by changing the direction of the toroidal magnetic field (from clockwise, looking down on the torus to counter-clockwise).[54] The standard, $-B_T$ or clockwise, direction was used in shot #142111 and produces modes that rotate in the ion diamagnetic direction (i.e., clockwise in the cross sections of Fig. 5) in both experiment and simulation.

The up-down asymmetry of the mode structure comes from radial symmetry-breaking, mainly by the radial variations of fast ion pressure gradients.[54] In the radially local (1D) theory, the ballooning mode has a radial structure characterized by $k_r = 0$ at a poloidal angle θ_0 (so-called

ballooning angle) because of the radial symmetry. In general, θ_0 is determined by local plasma parameters such as magnetic shear, the shear of diamagnetic flows and radial electric field. Any breaking of the radial symmetry, i.e., radial variations of pressure gradients, leads to the radial dependence of θ_0. Then, the radial mode structure can be twisted and a radially non-local (2D) eigenmode theory[61] is needed to solve the radial mode structure. In the current problem, the fast ion pressure gradient is the dominant source for the radial symmetry breaking, which ultimately determines the radial mode structure.[25,49–54] Therefore, fully self-consistent, non-perturbative simulation is needed to determine the eigenmode structure in order to accurately calculate the damping and growth rate.

V. VARIATION IN MODE STRUCTURES AS A FUNCTION OF q_{min}

Data from ECE Imaging has been used extensively in this study as it represents a powerful tool for unambiguously determining the structure of Alfvén eigenmodes in 2D, with localized and high-resolution measurement of fluctuating electron temperature. For relevant conditions, normalized δT_e is found to be an excellent proxy for potential fluctuations. The purpose of this section is to present further ECE data (from a separate better diagnosed discharge) that supports the trend, indicated in the previous section, for the mode structure to become more strongly ballooning as q_{min} decreases. A comparison of several modes from shot #142111 to the predictions of TAEFL was carried out in Ref. 25. In the course of this work, discrepancies between measured and simulated eigenmode frequency have been significantly reduced with the inclusion of acoustic effects in the TAEFL model. Furthermore, high-resolution spectrograms produced from ECEI data have allowed for evaluation of the RSAE growth rate. A fitting of the interpolated spectral line width to that produced by the model for a simple damped oscillator provides an estimate of the growth rate, and although error bars for this measurement are significant ($\pm 5\%$ of the real RSAE frequency), fractional growth rates are approximately 15% and trending toward smaller growth rates as frequency sweeps upward. This trend is readily apparent from the steadily decreasing RSAE mode amplitude and agrees qualitatively with simulations.[54]

Only a limited view of the eigenmode at the low field side of the magnetic axis is available from ECEI for shot #142111. However, in subsequent experimental campaigns, Alfvén eigenmodes have been imaged at both sides of the magnetic axis simultaneously using the dual-array capability of the DIII-D ECEI diagnostic.[25,62] The addition of 160 channels (8 radial $\times$ 20 vertical) at the high field side of the magnetic axis enables greater accuracy in the evaluation of the dominant poloidal mode number, better constrains the eigenmode phase, and reveals any ballooning (poloidal variation of mode amplitude on a flux surface) that may result from the mixing of poloidal sidebands (i.e., neighboring poloidal mode numbers). Resolution is improved at inboard radii, where the diagnostic must couple to high poloidal wavenumbers due to compression of the angular coordinate in a straight magnetic field line coordinate system, by adjusting zoom optics.

The most striking and readily resolved element of RSAE mode structure evolution with variation of q_{min} is the tendency of sweeping modes to become more ballooning (i.e., stronger poloidal variation) as their frequency approaches the TAE gap in the Alfvén continuum, consistent with the simulation results of Fig. 5. It was noted in Sec. IV that Alfvén eigenmode behavior is empirically insensitive to modest changes in plasma shape, and it has been shown in Ref. 54 that eigenmode phase characteristics are uniquely correlated to the direction of ion diamagnetic flow on DIII-D. Therefore, the lower single null discharge #144256, in which the toroidal magnetic field is in the reversed $+B_T$ direction, may be used without loss of generality to illustrate this ubiquitous feature. In Figure 6, the evolution of a typical $n=4$ RSAE is captured as the mode sweeps over nearly 40 kHz. Initially, the mode has uniform amplitude on any flux surface, and its structure is readily resolved at both sides of the magnetic axis. As the value of q_{min} falls and the mode sweeps up, however, the balance of amplitude at high and low field sides of the magnetic axis is lost, and the mode structure begins to resemble that of a TAE, with a strong

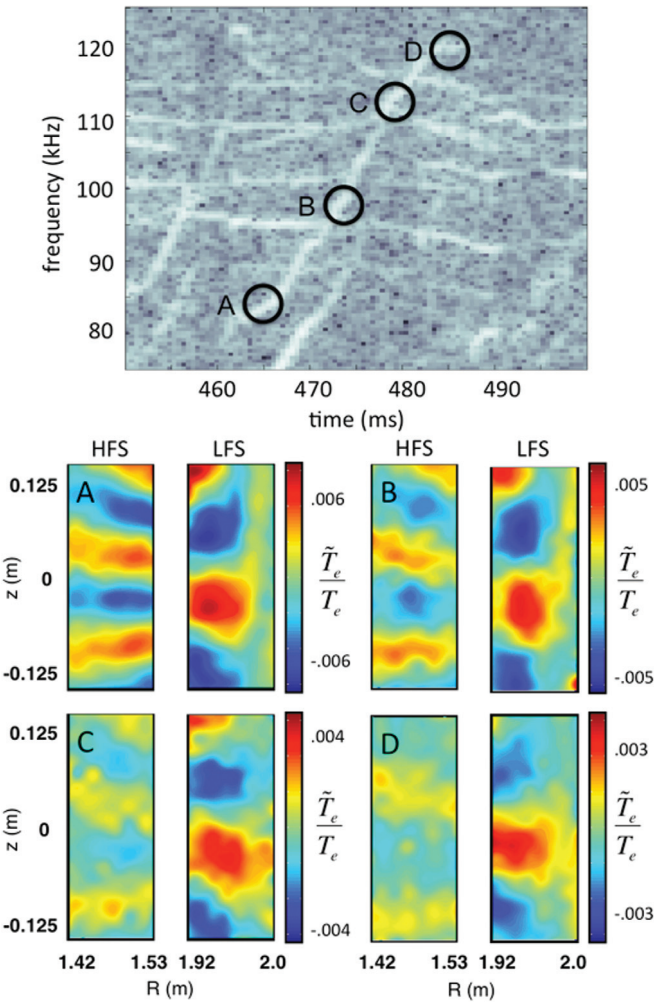

FIG. 6. Measurement of n = RSAE mode structure at selected times during the frequency sweep reveals the harmonic onset of ballooning character. The data shown is taken from shot #144256.

ballooning character which may be attributed to the beating of the dominant poloidal harmonic, m, with neighboring sidebands.

The vertical resolution of the ECEI diagnostic being approximately 2 cm with a total coverage of ~20 cm at high field radii, it is possible to make an accurate identification of the dominant poloidal mode number, along with direct observation of ballooning variation across the midplane. However, least squares fitting of ECEI data to a superposition of poloidal mode numbers does not adequately discriminate between $m+1$ and $m-1$ contributions, making a more detailed poloidal mode number decomposition such as shown for the simulated eigenmodes of Fig. 4 inherently arbitrary. Therefore, this level of detailed validation remains beyond the capabilities of current diagnostic techniques.

VI. CONCLUSIONS

An initial verification and validation study has been presented based on applying the two gyrokinetic codes GTC (Ref. 44) and GYRO (Ref. 55) and the gyro-Landau fluid model TAEFL (Ref. 57) to frequency sweeping RSAE/TAE instabilities that were observed[25,26] in DIII-D discharge #142111. These phenomena often occur in tokamak discharges with reversed shear q-profiles, an important regime for future steady-state tokamak operation. Considering the rather different physics representations and numerical solution techniques used in these separate models, good agreement is obtained between the different simulations with respect to the mode structure, growth rate, and real frequency as the q-profiles are scanned over a range of q_{min} values that characterize the experiment. Furthermore, the simulations reproduce the characteristic upward frequency sweep that is observed in the experiment as q_{min} decreases, including a slight drop-off in frequency at the lowest q_{min} values as the dominant mode transitions from an RSAE to a TAE instability. Doppler-shifted mode frequencies that are measured experimentally fall within $\sim\pm 8\%$ of the average of those predicted from the simulations and $\sim\pm 18\%$ from the individual simulations. This very predictable relation between q_{min} and frequency in discharges with reversed shear q-profiles is one of the features that motivate interest in Alfvén spectrum measurements as a q-profile diagnostic and in the general area of MHD spectroscopy. Since simple magnetic probe measurements can be employed, such techniques are of interest for future high neutron flux devices where other diagnostics may not be available. Both the predicted mode structures and experimental measurements show deviations from up-down symmetry that are driven by fast ion diamagnetic/perturbative effects. Unresolved differences with experiment and subtle variations amongst the codes remain. One of the most important variables for simulating EP-driven instabilities is the fast ion distribution function $f_{EP}(\mathbf{r},\mathbf{v})$. Currently, this is not well-diagnosed and more flexibility in the form of $f_{EP}(\mathbf{r},\mathbf{v})$ needs to be included in the models; anticipated future improvements in the measurement of $f_{EP}(\mathbf{r},\mathbf{v})$ will allow better validations of theory with experiment.

ACKNOWLEDGMENTS

This collaboration is supported by the US DOE SciDAC GSEP Center. Research has been sponsored by the US Department of Energy under Contract DE-AC05-00OR22725 with UT-Battelle, LLC; Cooperative Agreements DE-FC02-08ER54977 and DE-FC02-04ER54698 with General Atomics; DE-FC02-08ER54976 with UC Irvine, under DE-FG02-99ER54531, SC-G903402, DE-AC02-09CH11466, DE-AC05-00OR22725, and DE-FC-02-04ER54698 for the UC Davis/ECEI collaboration; and under DE-FG03-97ER54415 with the University of Texas at Austin. Further support was provided by NRF-201100187244, Korea, and the Association EURATOM-FOM. This research used resources of the National Energy Research Scientific Computing Center, which is supported by the Office of Science of the U.S. Department of Energy under Contract No. DE-AC02-05CH11231. Also, the resources of the Oak Ridge Leadership Computing Facility, located in the National Center for Computational Sciences at Oak Ridge National Laboratory, which is supported by the Office of Science of the Department of Energy under Contract DE-AC05-00OR22725, were used.

[1]W. L. Oberkampf, T. G. Trucano, and C. Hirsch, Appl. Mech. Rev. **57**, 345 (2004).
[2]P. W. Terry, M. Greenwald, J.-N. Leboeuf, G. R. McKee, D. R. Mikkelsen, W. M. Nevins, D. E. Newman, and D. P. Stotler, Phys. Plasmas **15**, 062503 (2008).
[3]M. Greenwald, Phys. Plasmas **17**, 058101 (2010).
[4]C. Kessel, J. Manickam, G. Rewoldt, and W. M. Tang, Phys. Rev. Lett. **72**, 1212 (1994).
[5]F. W. Perkins, A. Bondeson, R. J. Buttery, J. D. Callen, J. W. Connor *et al.*, Nucl. Fusion **39**, 2051 (1999).
[6]T. Fujita, S. Ide, H. Shirai, M. Kikuchi, O. Naito, Y. Koide, S. Takeji, H. Kubo, and S. Ishida, Phys. Rev. Lett. **78**, 2377 (1997).
[7]S. Takeji, S. Tokuda, T. Fujita, T. Suzuki, A. Isayama, S. Ide, Y. Ishii, Y. Kamada, Y. Koide, T. Matsumoto, T. Oikawa, T. Ozeki, and Y. Sakamoto, Nucl. Fusion **42**, 5 (2002).
[8]C. M. Greenfield *et al.*, Phys. Plasmas **11**, 2616 (2004).
[9]X. Litaudon *et al.*, Plasma Phys. Controlled Fusion **44**, 1057 (2002).
[10]S. Ide *et al.*, Nucl. Fusion **40**, 445 (2000).
[11]A. Sips, J. Hobirk, A. G. Peeters, Fusion Sci. Technol. **44**, 605 (2003).
[12]M. Porkolab, P. T. Bonoli, Y. Lin, S. J. Wukitch, C. Fiore *et al.*, AIP Conf. Proc. **694**, 162 (2003).
[13]C. Gormezano, A. C. C. Sips *et al.*, Nucl. Fusion **47**, S285–S336 (2007).
[14]Kimura *et al.*, Nucl. Fusion **38**, 1303–1314 (1998).
[15]S. Sharapov *et al.*, Phys. Lett. A **289**, 127–134 (2001).
[16]R. Nazikian, G. J. Kramer, C. Z. Cheng, and N. N. Gorelenkov, Phys. Rev. Lett. **91**, 125003 (2003).
[17]J. Snipes, N. Basse, C. Boswell, E. Edlund, A. Fasoli, N. N. Gorelenkov, R. S. Granetz, L. Lin, Y. Lin, R. Parker, M. Porkolab, J. Sears, S. Sharapov, V. Tang, and S. Wukitch, Phys. Plasmas **12**, 056102 (2005).
[18]M. A. Van Zeeland, G. J. Kramer, R. Nazikian, H. L. Berk, T. N. Carlstrom, and W. M. Solomon, Plasma Phys. Controlled Fusion **47**, L31–L40 (2005).
[19]E. Fredrickson, N. A. Crocker, N. N. Gorelenkov, W. W. Heidbrink, S. Kubota, F. M. Levinton, H. Yuh, J. E. Menard, and R. E. Bell, Phys. Plasmas **14**, 102510 (2007).
[20]B. N. Breizman, H. L. Berk, and M. S. Pekker, Phys. Plasmas **10**, 3649 (2003).
[21]B. N. Breizman and M. S. Pekker, Phys. Plasmas **12**, 112506 (2005).
[22]H. L. Berk, B. N. Breizman, and N. V. Petviashvili, Phys. Lett. A **234**(3), 213 (1997).
[23]R. B. White, N. Gorelenkov, W. W. Heidbrink, and M. A. Van Zeeland, Plasma Phys. Controlled Fusion **52**, 045012 (2010).
[24]R. B. White, N. Gorelenkov, W. W. Heidbrink, and M. A. Van Zeeland, Phys. Plasma **17**, 056107 (2010).
[25]B. Tobias, I. G. J. Classen, C. W. Domier, W. W. Heidbrink, N. C. Luhmann, Jr., R. Nazikian, H. K. Park, D. Spong, and M. A. Van Zeeland, Phys. Rev. Lett. **106**, 075003 (2011).

[26]B. J. Tobias, R. L. Boivin, J. E. Boom, I. G. J. Classen, C. W. Domier, A. J. H. Donné, W. W. Heidbrink, N. C. Luhmann, Jr., T. Munsat, C. M. Muscatello, R. Nazikian, H. K. Park, D. A. Spong, A. D. Turnbull, M. A. Van Zeeland, G. S. Yun, and DIII-D Team, Phys. Plasmas **18**, 056107 (2011).
[27]See http://phoenix.ps.uci.edu/gsep/
[28]E. M. Carolipio, W. W. Heidbrink, C. Z. Cheng, M. S. Chu, G. Y. Fu, A. Jaun, D. A. Spong, A. D. Turnbull, and R. B. White, Phys. Plasmas **8**, 3391 (2001).
[29]M. A. Van Zeeland, G. J. Kramer, M. E. Austin *et al.*, Phys. Rev. Lett. **97**, 135001 (2006).
[30]M. A. Van Zeeland, M. E. Austin, N. N. Gorelenkov *et al.*, Phys. Plasma **14**, 056102 (2007).
[31]M. A. Van Zeeland, W. W. Heidbrink, R. Nazikian *et al.*, Nucl. Fusion **49**, 065003 (2009).
[32]C. Z. Cheng, Phys. Rep. **211**, 1 (1992).
[33]W. W. Heidbrink, N. N. Gorelenkov, Y. Luo *et al.*, Phys. Rev. Lett. **99**, 245002 (2007).
[34]W. W. Heidbrink, M. A. Van Zeeland, M. E. Austin *et al.*, Nucl. Fusion **48**, 084001 (2008).
[35]D. C. Pace, R. K. Fisher, M. Garcia-Munoz, W. W. Heidbrink, and M. A. Van Zeeland, Plasma Phys. Controlled Fusion **53**, 062001 (2011).
[36]M. A. Van Zeeland, W. W. Heidbrink, R. K. Fisher, M. Garcia Munoz *et al.*, Phys. Plasmas **18**, 056114 (2011).
[37]L. L. Lao, H. St. John, R. D. Stambaugh, A. G. Kellman, and W. Pfeiffer, Nucl. Fusion **25**, 1611 (1985).
[38]B. W. Rice, D. G. Nilson, and D. Wroblewski, Rev. Sci. Instrum. **66**, 373 (1995).
[39]S. E. Sharapov, B. Alper, H. L. Berk *et al.*, Phys. Plasma **9**, 2027 (2002).
[40]A. Pankin, D. Mccune, R. Andre, G. Bateman, and A. Kritz, Comput. Phys. Commun. **159**, 157 (2004).
[41]Z. Lin, T. S. Hahm, W. W. Lee, W. M. Tang, and R. B. White, Science **281**, 1835 (1998).
[42]R. B. White and M. S. Chance, Phys. Fluids **27**, 2455 (1984).
[43]A. Brizard and T. S. Hahm, Rev. Mod. Phys. **79**, 421–468 (2007).
[44]I. Holod, W. L. Zhang, Y. Xiao, and Z. Lin, Phys. Plasmas **16**, 122307 (2009).
[45]W. W. Lee, J. Comput. Phys. **72**, 243 (1987).
[46]Y. Xiao and Z. Lin, Phys. Plasmas **18**, 110703 (2011).
[47]I. Holod, Z. Lin, and Y. Xiao, Phys. Plasmas **19**, 012314 (2012).
[48]W. Zhang, V. Decyk, I. Holod, Y. Xiao, Z. Lin, and L. Chen, Phys. Plasmas **17**, 055902 (2010).
[49]W. Deng, Z. Lin, I. Holod, X. Wang, Y. Xiao, and W. Zhang, Phys. Plasmas **17**, 112504 (2010).
[50]H. S. Zhang, Z. Lin, I. Holod, X. Wang, Y. Xiao, and W. L. Zhang, Phys. Plasmas **17**, 112505 (2010).
[51]W. Zhang, I. Holod, Z. Lin, and Y. Xiao, Phys. Plasmas **19**, 022507 (2012).
[52]W. Deng, Z. Lin, and I. Holod, Nucl. Fusion **52**, 023005 (2012).
[53]W. W. Lee, J. Comput. Phys. **72**, 243 (1987).
[54]W. Deng, Z. Lin, I. Holod, Z. Wang, Y. Xiao, and H. Zhang, Nucl. Fusion **52**, 043006 (2012).
[55]J. Candy and R. E. Waltz, J. Comput. Phys. **186**, 545 (2003).
[56]E. M. Bass and R. E. Waltz, Phys. Plasmas **17**, 112319 (2010).
[57]D. A. Spong, B. A. Carreras, and C. L. Hedrick, Phys. Fluids B **4**, 3316 (1992).
[58]D. A. Spong, B. A. Carreras, and C. L. Hedrick, Phys. Plasmas **1**, 1503 (1994).
[59]G. W. Hammett and F. W. Perkins, Phys. Rev. Lett. **64**, 3019 (1990).
[60]L. A. Charlton, J. A. Holmes, H. R. Hicks, V. E. Lynch, and B. A. Carreras, J. Comput. Phys. **63**, 107 (1986).
[61]F. Romanelli and F. Zonca, Phys. Fluids B **5**, 4081 (1993).
[62]B. Tobias, C. Domier, T. Liang, X. Kong, L. Yu, G. Yun, H. Park, I. G. J. Classen, J. Boom, and A. Donnè, Rev. Sci. Instrum. **81**, 10D928 (2010).